# Continuous Cooling Transformation Diagrams of HSLA Steel for Seamless Tubes Production

**Ivo Schindler[a], Rostislav Kawulok[a], Yann Seillier[a], Petr Kawulok[a], Petr Opěla[a], Stanislav Rusz[a], Vlastimil Vodárek[a], Rostislav Turoň[b]**

*[a] VŠB – Technical University of Ostrava, Faculty of Materials Science and Technology, Ostrava-Poruba, Czech Republic, e-mail: ivo.schindler@vsb.cz, rostislav.kawolok@vsb.cz, seillier.yann@gmail.com, petr.kawulok@vsb.cz, petr.opela@vsb.cz, stanislav.rusz2@vsb.cz, vlastimil.vodarek@vsb.cz*

*[b] TŘINECKÉ ŽELEZÁRNY a.s., Třinec, Czech Republic, e-mail: Rostislav.Turon@trz.cz*

**(Received 17 December 2018; accepted 29 April 2019)**

**Abstract**

The CCT and two DCCT diagrams were constructed for the HSLA steel containing Cr, V, Nb and N microadditions, taking into account industrial processing parameters of this material in a seamless tubes rolling mill. The typical finish hot rolling temperature of 1173 K was used for the construction of the standard CCT diagram and the effect of previous austenite deformation at this temperature was evaluated in the DCCT diagram. Another DCCT diagram was developed after heating at 1553 K, followed by plastic deformation at 1173 K. The prior austenite grain size in the hot rolled material after heating at 1173 K was approx. 10 μm, heating of the as-cast material at 1553 K resulted in the prior austenite grain size over 200 μm. The effect of previous austenite deformation after low-temperature heating on the CCT diagram was negligible. The high-temperature heating showed a great influence on the austenite decomposition processes. The Ferrite-start temperature was significantly reduced at high cooling rates and the preferred decomposition of coarse grained austenite to acicular ferrite suppressed the bainite transformation at medium cooling rates. The developed DCCT diagrams can be used for the prediction of austenite decomposition products during cooling of the seamless tubes from the finish rolling temperature. The CCT diagram can be utilized for the quality heat treatment of tubes.

**Key words:** HSLA steel; seamless tubes rolling; dilatometry; deformation CCT diagram; austenite decomposition processes.

## 1. INTRODUCTION

The key role in optimization of the structure and mechanical properties of hot rolled metallic materials is played not only by the history of forming (i.e. various controlled rolling procedures, etc.) but also by the parameters of final cooling [1-3]. The final cooling rate makes it possible to control the austenite softening processes, phase transformations during decomposition of austenite and grain growth. The published results [4-12], and our experiences gained in the laboratory conditions using the hot deformation simulator Gleeble 3800 [13-14] as well as the semi-continuous hot rolling mill [15-16] prove the crucial role of the cooling parameters after hot forming. This can be deduced from the continuous cooling transformation diagrams, especially when considering the previous deformation history. Recently, thanks to two dilatometer systems available on the Gleeble simulator, the researchers of the VŠB-TUO have created continuous cooling transformation diagrams for a number of chemically very

different steel grades in the traditional version (CCT) as well as after the previous deformation of austenite (DCCT) – see [17, 18] for example. The effect of austenite deformation is very complex and manifests itself differently, e.g. by refining the prior austenite grains due to static recrystallization or by the modification of the austenite decomposition kinetics as a result of deformation strengthening.

Deformation of austenite accelerates its decomposition to ferrite and pearlite (diffusion-controlled transformations) [5, 19, 20]. The energy accumulated by plastic deformation below the recrystallization stop temperatures represents the significant driving force for allotriomorphic ferrite nucleation. According to Khlestov et al. [21], deformation accelerates the start of diffusion-controlled transformations and this effect grows with increasing deformation. The interval between $A_{r1}$ and $A_{r3}$ temperatures is narrowed up to the true strain of 0.4. This results in a significant acceleration of pearlitic transformation [22]. Deformation increases density of lattice defects in austenite. It enhances diffusion processes in the solid solution and increases the nucleation rate of the products of diffusional decomposition of austenite. The nucleation rate is high, however the mobility of phase interfaces is severely decelerated by a high density of dislocations in austenite and that is why the final fraction of ferrite decreases. In the case of very large plastic deformation, the high nucleation rate compensates the slow growth of nuclei and the resulting ferrite fraction is approximately the same as in the case of austenite not affected by plastic deformation; however, the ferrite grains are much finer [17, 23-28].

The effect of austenite plastic deformation on the bainitic transformation kinetics depends strongly on the deformation value and especially on the chemical composition of the steel. Bainitic transformation is accompanied by two contradictory phenomena in deformed austenite. The nucleation rate of nuclei is high and the bainitic ferrite starts to develop in the form of narrow laths decorated by carbides. At the same time the lath growth is limited which results in a repeated nucleation of bainitic ferrite laths. Furthermore, the growth rate of nuclei may be affected by the deformation induced precipitation of MX particles in austenite, which act as obstacles for the movement of phase interfaces. If the deformation takes place during the austenite→bainite transformation, the kinetics of decomposition is significantly accelerated [22, 29-34]. Results of Yi et al. [34] investigations on the kinetics of bainite transformation in a micro-alloyed steel show that the bainite start temperature $B_S$ rise is affected by the both heating temperature and the amount of plastic deformation in the area of stable austenite, especially in the case of deformation at lower temperatures (1223 K). At the increased deformation temperature (1273 K), the effect of plastic deformation on the $B_S$ rise is practically negligible. This can be attributed to a sufficient pause between the deformation and the decomposition of austenite during which the deformed austenite can be significantly restored and thus the effect of the prior deformation can be suppressed.

Deformation of austenite usually results in a rise of the martensite start temperature $M_S$ [5, 22, 29, 35]. The $M_S$ temperature increases with the plastic deformation value up to the limit temperature reported as Md. Deformation induced precipitation of MX particles in austenite can have the similar effect on the $M_S$ temperature. This is the result of a reduction of the carbon content in austenite.

Furthermore, microstructure characteristics at the beginning of cooling (from the finish rolling temperature, or from the austenitization temperature at the dilatometer test) are very important. First of all the prior austenite grain size may significantly affect the austenite decomposition processes [29, 36]. The kinetics of diffusion-controlled transformations strongly depends on the prior austenite grain size since decomposition of austenite starts at grain boundaries. The total area of grain boundaries per unit volume of austenite increases as the grain size decreases. Fine austenite grains provide more potential sites for nucleation of ferrite which results in acceleration of transformation [5]. Farrar et al. [37] investigations support the above described theory. The reduction of the prior austenite grain size (32 μm, 93 μm and 208 μm) initiated the ferrite transformation of the low carbon Mn–Ni steel at higher temperatures. Coarse austenite grains suppress the formation of allotriomorphic (polygonal) ferrite and

at same time support the formation of Widmanstätten ferrite and acicular ferrite. The control of the prior austenite grain size before the austenite decomposition represents a critical factor from the point of view of the resulting microstructure and mechanical properties of hot formed steels.

Similarly, the prior austenite grain size plays a very important role in the kinetics of austenite →pearlite transformation. The pearlite transformation starts with the formation of either ferrite or cementite nuclei at the austenite grain boundaries. The nucleation rate of pearlite is accelerated as the prior austenite grain size decreases [5, 38]. According to Nürnberger et al. [5] the dependence between the time for the ferrite transformation start as well as the time for the start and finish of pearlite transformation and the ASTM austenite grain size is almost linear in the semi-log plot. Furthermore, slope of lines for the Ferrite-start (Fs), Pearlite-start (Ps) and Pearlite-finish (Pf) temperatures in this plot is approximately the same.

Some studies did not prove any significant effect of the prior austenite grain size on the bainite transformation. However, in some steels a drop in the austenitization temperature resulted in a reduction of the bainite transformation rate [39-41]. The coarsening of prior austenite grains leads to rise in the Martensite-start (Ms) temperature [39, 42]. A similar effect of the prior austenite grain size is also assumed for the temperature of the end of martensitic transformation Mf. The prior austenite grain size also affects the morphology of martensite. The length of martensitic laths increases with the prior austenite grain size [42, 43].

Transformation diagrams are mostly constructed after heating of the material directly on a relatively low austenitization temperature. This is justified in the technological practice when relatively fine-grained microstructure enters into the final cooling phase. However, it is the subject of interest how is the kinetics of austenite decomposition affected in the case of austenitization at a high temperature, followed by rolling with a relatively small total strain at a relatively high finish rolling temperature. A typical example of such technology may be the traditional production of thick-walled seamless tubes by the Mannesmann process combining the piercing of the billet or bloom by diagonal rolling with the subsequent elongating of the hollow semi-finished product on the Pilgrim tube-rolling mill [44]. Therefore, the main objective of this paper is the construction of three continuous cooling transformation diagrams for an HSLA steel intended for the seamless tubes production. The aim is to identify the combined effect of the initial microstructure and previous austenite deformation on the temperatures and kinetics of austenite decomposition processes in the wide range of cooling rates.

## 2. EXPERIMENTAL

Experimental material was supplied in the form of continuously cast round bloom with the diameter of 400 mm. Chemical composition of the tested HSLA steel was as follows: 0.16 C – 1.05 Mn – 0.20 Si – 0.19 Cr – 0.031 Nb – 0.046 V – 0.0093 N (in weight %) Two sets of specimens were taken from this bloom [45]. Dilatometer specimens with a coarse-grained structure were made intentionally from the part of columnar crystals – see **Fig. 1**. The reason was the effort to simulate the specific technological parameters of the seamless tubes rolling. The adoption of a structure formed by columnar crystals is very close to the operating conditions and makes a contribution to the applied research in TŘINECKÉ ŽELEZÁRNY plant. Prior austenite grain boundaries were revealed by etching at a room temperature using a saturated aqueous picric acid solution with a wetting agent. The as-quenched specimens had to be annealed at the temperature of 693 K for 2 hours in advance. Conventional metallographic examination by light microscopy was used for the microstructure analysis of all specimens. The grain size calculation was based on the intercept lengths measurement with the software QuickPHOTO INDUSTRIAL 3.2 (PROMICRA s.r.o.).

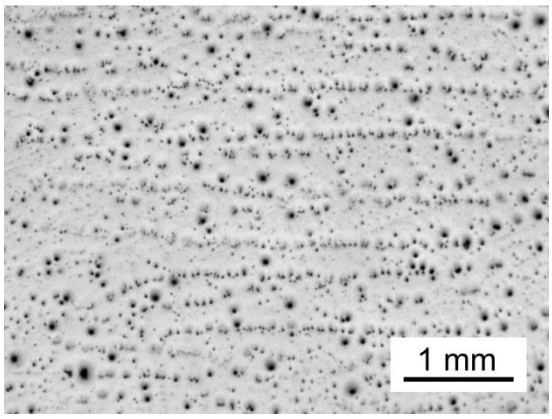


**a)** columnar crystals, polished state

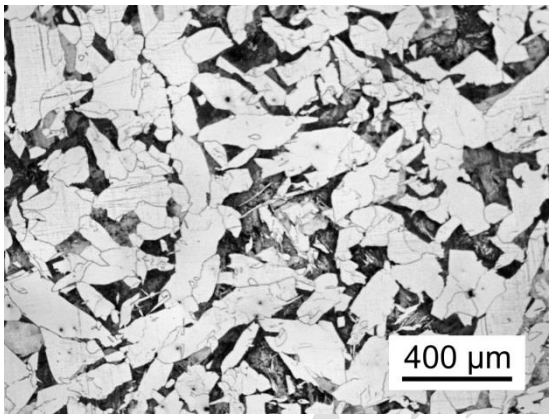


**b)** coarse grained microstructure formed by a mixture of ferrite and pearlite

**Fig. 1** Microstructure of the bloom in the area of columnar crystals

Prisms with the cross-section of 70 x 70 mm were cut out from the middle part of bloom with equiaxed crystals. These prisms were hot rolled on the reversing stand (more specifically on the plane part of the rolls with the diameter of 350 mm) from the height of 70 mm to plate with the thickness of 8.5 mm. The prism was preheated in an electric resistance furnace to the temperature of 1523 K and then it was flat rolled in 10 passes to the thickness of 25 mm. After reheating to 1523 K again, rolling was completed in 6 passes with the final rolling temperature of approx. 1213 K. This was followed by normalizing annealing at the temperature of 1173 K resulting in a very fine microstructure (see **Fig. 2**) – mean size of ferritic grain was approx. 8 µm.

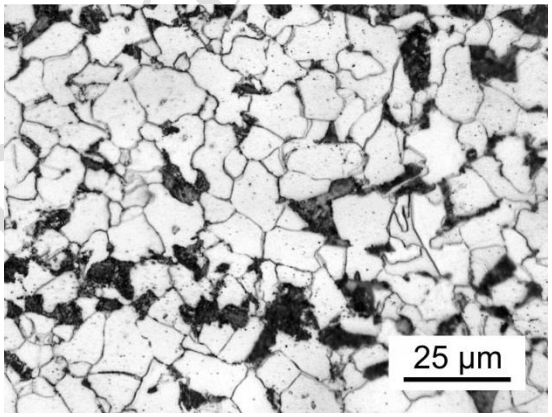


**Fig. 2** Fine-grained ferrite and pearlite microstructure after hot rolling and normalizing annealing

Longitudinal axes of the cylindrical dilatometer specimens were oriented parallel to the casting direction (for the continuously cast bloom) or to the flat rolling direction (in the case of the laboratory rolled plates). Cylindrical specimens of Ø 6 x 86 mm made from the fine-grained material were used for dilatometer test after austenitization at 1173 K / 180 s. The identical specimens made from the coarse-grained material were used for the testing after heating at 1553 K / 300 s. This high-temperature heating corresponds to the technology of piercing of bloom at the seamless tube rolling mill and it leads to dissolving of carbides and nitrides of micro-alloying elements [42]. By etching the prior austenitic grains

boundaries in the heated and quenched specimens it was possible, at least for orientation, to identify their parameters – mean size over 200 μm after high-temperature heating, or 10 μm after low temperature heating (see **Fig. 3**).

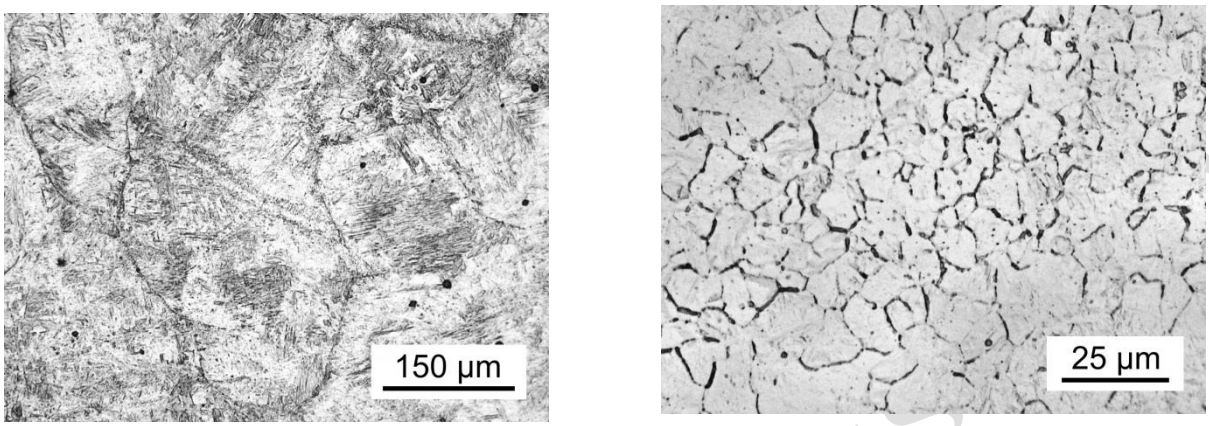


**a)** 1553 K **b)** 1173 K

**Fig. 3** Effect of the heating temperature on the prior austenite grain size

The dilatometer tests associated with the DCCT diagrams could be performed with the cooling rate of 0.15 – 80 $K \cdot s^{-1}$. Higher rates (up to 180 $K \cdot s^{-1}$) were achieved in the case of tests without deformation using specimens with hollow head and reduced central part with size of Ø 5 x 5 mm.

The Model 39018 CCT Dilatometer was used on the Gleeble 3800 system (Dynamic Systems Inc.) for the measuring of all phase transformation temperatures. It is an LVDT based dilatometer system with quartz contact tips. This system is rated for the continuous operation in the temperature range of 284 K – 1573 K which can be for a limited operation time extended up to 1673 K. The dilatometer has the resolution of ± 0.4 μm and linearity of ± 0.25 % in the full scale of ± 2.5 mm. An applied strain rate is limited to the value of 40 $s^{-1}$. The Model 39112 Scanning Non-Contact Optical Dilatometer System (Dynamic Systems Inc.) with repeatability of ± 0.3 μm was used only marginally for some comparative tests because it can work only at the maximum temperature of 1473 K. Location of the transformation temperatures was detected by the dilatation curves analysis in two steps. First, points of deviation from the linear shape were determined semi-automatically in the CCT software (Dynamic Systems Inc.). Subsequently, the results were verified and specified by the analysis of the first derivative of raw curves. The Origin software (OriginLab Corp.) was utilized to gently smooth some noisy data and differentiate the curves (using the Savitzky-Golay smoothing).

Based on the dilatometer tests in combination with metallographic analyses and HV 30 hardness measuring, the CCT (1173 K) and also DCCT (1173 K) diagrams were created after the low-temperature austenitization, and after the high-temperature heating only DCCT (1553 K) diagram was developed. True (logarithmic) compression strain with the value of 0.35 was performed by uniaxial compression with the strain rate of 1 $s^{-1}$. The scheme of the dilatometer experiment with the high-temperature heating is shown in **Fig. 4**. Of course, for the transformation diagram creation it was necessary to deduct to time periods before the proper cooling from 1173 K, otherwise the individual diagrams would not be comparable.

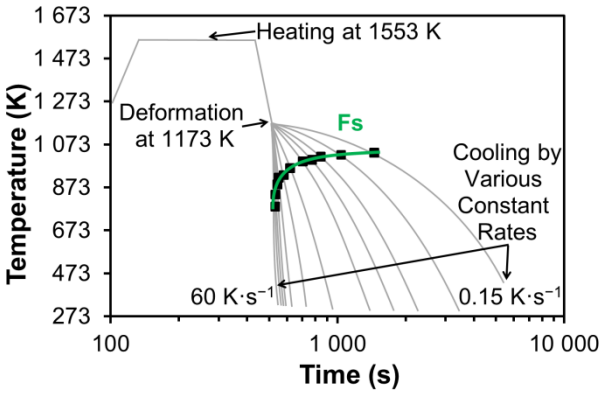


**Fig. 4** Scheme of the dilatometer tests after heating at 1553 K

Microstructure of specimens subjected to dilatometer tests was revealed by etching in Nital (2% $HNO_3$ in alcohol). Quantitative evaluation of austenite decomposition products in the individual specimens was carried out by the point counting method. Ten light microscopy micrographs at the same magnification (500x) were analyzed for each specimen. The following phases and microstructure constituents were distinguished: F = polygonal (allotriomorphic) ferrite, AF = acicular ferrite, P = pearlite, GB = granular bainite, B = bainite and M = martensite. Light microscopy does not allow reliable distinction between martensite and bainite. Both constituents were quantitatively evaluated together (martensite + bainite). Granular bainite consists of bainitic ferrite and islands of the M/A constituent. In specimens containing coarse M/A blocks, this constituent was evaluated separately.

## 3. RESULTS

### 3.1. Microstructure evaluation after dilatometer tests

Metallographic investigations revealed that only after the slowest cooling rates microstructure consisted of a mixture of polygonal ferrite and pearlite. In specimens manufactured from the hot rolled plate pearlite colonies were arranged in bands parallel to the hot rolling direction – see **Fig. 5**. In specimens after heating at 1553 K two morphologies of ferrite were observed after cooling at the rates over 0.5 $K \cdot s^{-1}$. **Figure 6** shows a mixture of polygonal ferrite, acicular ferrite and pearlite in the specimen cooled at the constant rate of 0.7 $K \cdot s^{-1}$. The coarse prior austenite grain size preferred decomposition of austenite to acicular ferrite at the expense of bainitic transformation. At medium cooling rates granular bainite containing the M/A constituent was present in the final microstructure. In specimens heated at 1173 K the M/A constituent formed relatively coarse islands. On the other hand, in specimens heated at 1553 K granular bainite usually consisted of narrow laths of ferritic bainite mixed with fine islands of the M/A constituent. Intensive cooling from the heating temperature resulted in the formation of a mixture of bainite and martensite – see **Figs. 7** and **8**. The increase of hardness with the cooling rate rise proved that the fraction of martensite in the microstructure increased with the cooling rate. Nevertheless, even in specimens cooled with the fastest rates traces of allotriomorphic (polygonal) ferrite were present.

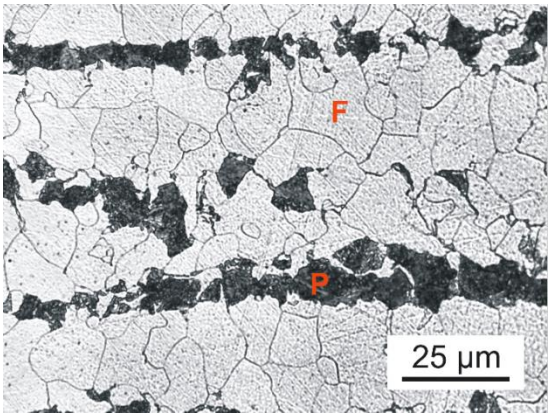


**Fig. 5** Banded ferrite and pearlite microstructure; CCT diagram – heating at 1173 K, cooling rate of 0.15 $K \cdot s^{-1}$

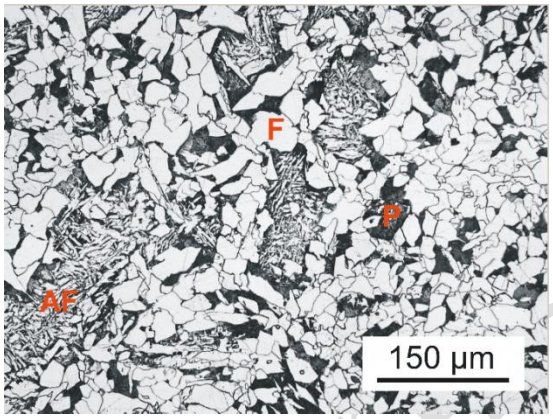


**Fig. 6** Microstructure formed by a mixture of equiaxed ferrite, pearlite and acicular ferrite; DCCT diagram – heating at 1553 K, cooling rate of 0.7 $K \cdot s^{-1}$

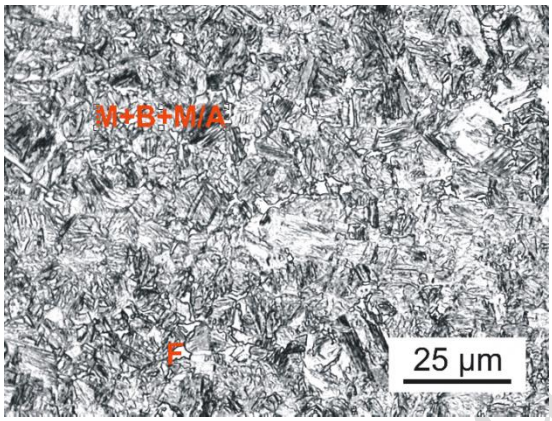


**Fig. 7** Microstructure formed by a mixture of martensite and bainite, the M/A component and a small fraction of polygonal ferrite; CCT diagram – heating at 1173 K, cooling rate of 180 $K \cdot s^{-1}$

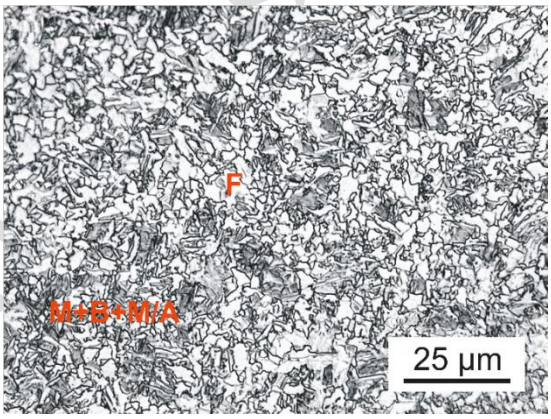


**Fig. 8** Microstructure consisting of a mixture of martensite and bainite, the M/A component and polygonal ferrite; DCCT diagram – heating at 1173 K, cooling rate of 80 $K \cdot s^{-1}$

The comparative **Fig. 9** demonstrates the microstructure evolution for all three transformation diagrams at the cooling rates of 4 $K \cdot s^{-1}$ and 35 $K \cdot s^{-1}$. Micrograph in Fig. 9a shows a mixture of ferrite, pearlite and islands of the M/A constituent in the specimen heated at 1173 K. Austenite deformation at 1173 K resulted in a higher fraction of the M/A constituent (granular bainite) in the microstructure (Fig. 9b). After heating at 1553 K, followed by plastic deformation at 1173 K and subsequent cooling at the rate of 4 $K \cdot s^{-1}$, austenite preferably decomposed to a mixture of ferrite, pearlite and granular bainite at the expense of allotriomorphic ferrite (Fig. 9c). Cooling of dilatometer specimens with the same thermal and deformation history as in Figs. 9a – c at the constant rate of 35 $K \cdot s^{-1}$ preferred the austenite decomposition to a mixture of bainite and martensite at the expense of diffusional transformation products (ferrite, pearlite – Figs. 9d – f).

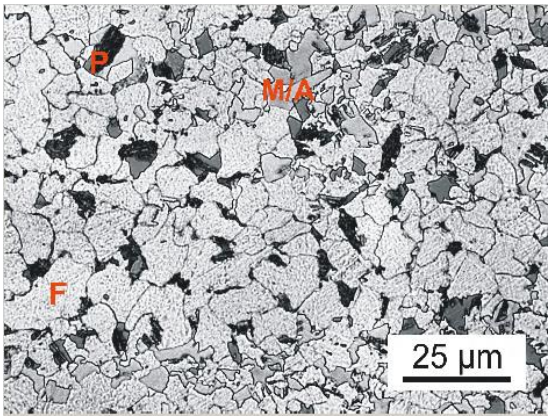


**a)** CCT (heating at 1173 K, cooling 4 K·s$^{-1}$)

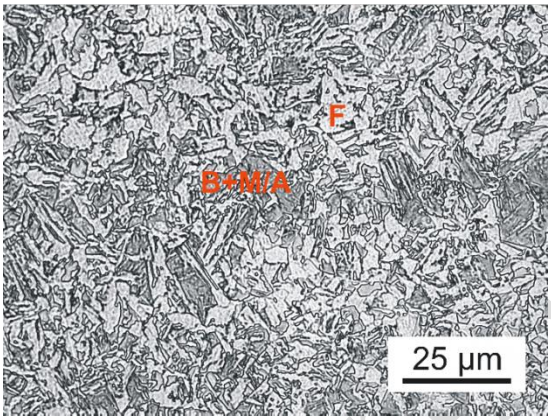


**d)** CCT (heating at 1173 K, cooling 35 K·s$^{-1}$)

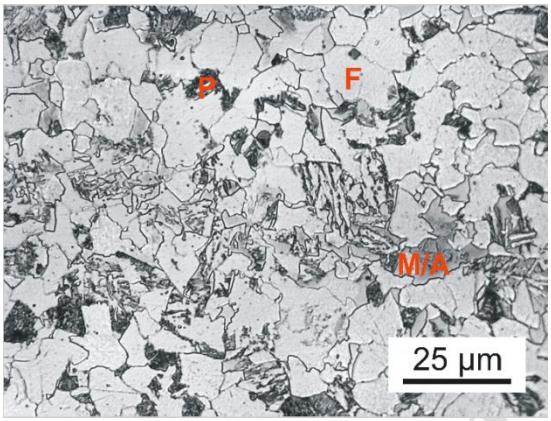


**b)** DCCT (heating at 1173 K, cooling 4 K·s$^{-1}$)

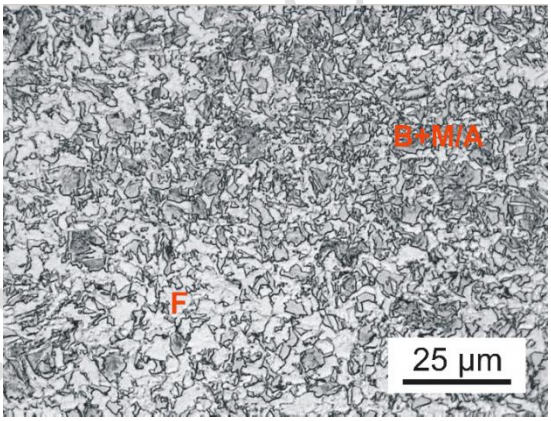


**e)** DCCT (heating at 1173 K, cooling 35 K·s$^{-1}$)

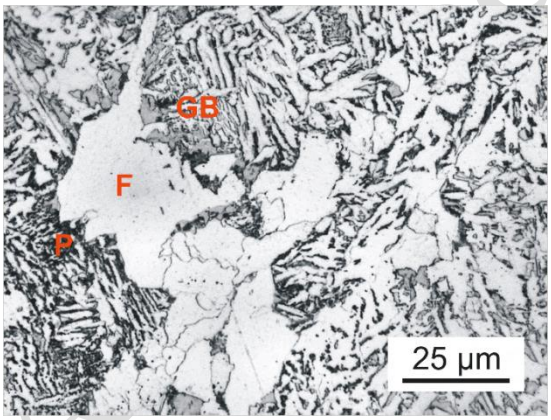


**c)** DCCT (heating at 1553K, cooling 4 K·s$^{-1}$)

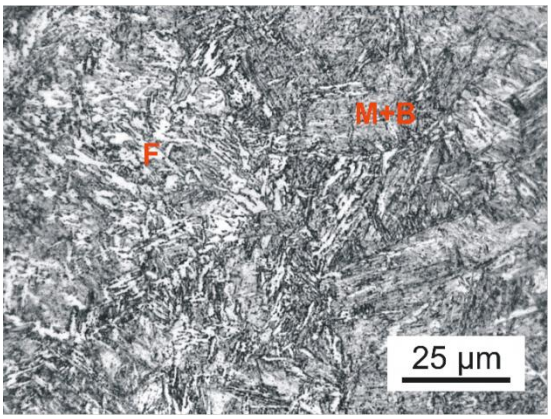


**f)** DCCT (heating at 1553K, cooling 35 K·s$^{-1}$)

**Fig. 9** Comparison of typical microstructure of the dilatometer specimens

### 3.2. Quantitative metallography and hardness evaluation

The summary of the mean values of hardness HV 30 and qualitative identification of the phases and microstructure constituents in individual specimens used for the construction of continuous cooling transformation diagrams is shown in **Tabs. 1-3**. As expected, diffusion-controlled transformation

products of austenite decomposition in specimens cooled at the very low cooling rates are associated with the lowest hardness level. The formation of acicular ferrite in specimens heated at 1553 K resulted in the higher hardness values in comparison with the specimens heated at 1173 K and cooled at the same cooling rates. The increasing fractions of granular bainite (the M/A constituent), bainite and martensite in the final microstructure are associated with a gradual increase in hardness values.

**Tab. 1** The effect of cooling rate on hardness and fractions of austenite decomposition products – CCT diagram, heating at 1173 K

| Cooling rate ($K \cdot s^{-1}$) | Hardness HV 30 | Microstructure | F (%) | P + M/A (%) | M + B + M/A (%) |
|---|---|---|---|---|---|
| 0.15 | 147 | F + P | 78 | 22 | - |
| 1 | 162 | F + P + M/A | 76 | 24 | - |
| 4 | 168 | F + P + M/A | 74 | 26 | - |
| 12 | 200 | F + P + M/A | 61 | 39 | - |
| 35 | 264 | F + M + B + M/A | 42 | - | 58 |
| 80 | 300 | F + M + B + M/A | 28 | - | 73 |
| 180 | 437 | F + M + B | 5 | - | 95 |

**Tab. 2** The effect of cooling rate on hardness and fractions of austenite decomposition products – DCCT diagram, heating at 1173 K

| Cooling rate ($K \cdot s^{-1}$) | Hardness HV 30 | Microstructure | F (%) | P + M/A (%) | M + B + M/A (%) |
|---|---|---|---|---|---|
| 0.15 | 147 | F + P | 79 | 21 | - |
| 0.5 | 151 | F + P | 77 | 23 | - |
| 4 | 174 | F + P | 68 | 32 | - |
| 12 | 221 | F + P + M/A | 54 | 46 | - |
| 35 | 238 | F + M + B + M/A | 45 | - | 55 |
| 80 | 266 | F + M + B + M/A | 32 | - | 68 |

**Tab. 3** The effect of cooling rate on hardness and fractions of austenite decomposition products – DCCT diagram, heating at 1553 K

| Cooling rate ($K \cdot s^{-1}$) | Hardness HV 30 | Microstructure | F (%) | P + M/A (%) | M + B + M/A (%) |
|---|---|---|---|---|---|
| 0.3 | 147 | F + P | 68 | 32 | - |
| 0.5 | 162 | F + AF + P | 65 | 35 | - |
| 0.7 | 168 | F + AF + P | 62 | 38 | - |
| 1 | 200 | F + AF + P | 60 | 40 | - |
| 4 | 264 | F + AF + GB | 52 | 48 | - |
| 12 | 300 | F + AF + GB | 40 | 60 | - |
| 20 | 437 | F+ AF + M + B | 20 | - | 80 |
| 35 | 389 | F + M + B | 5 | - | 95 |
| 60 | 413 | F + M + B | 1 | - | 99 |

The dependences of quantitative metallography results and hardness values HV 30 on the cooling rate are for individual continuous cooling transformation diagrams graphically represented in **Figs. 10 a-c**. It is evident that the most pronounced increase in hardness is associated with the formation of bainite and martensite. The kinetics of the formation of these microstructure constituents in the CCT (1173 K) and DCCT (1173 K) diagrams was slower than that in the DCCT (1553 K) diagram.

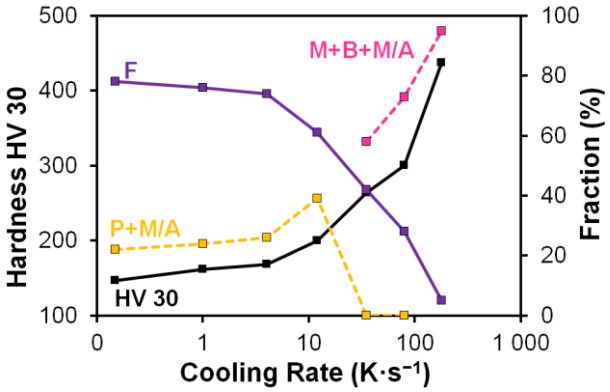


**a)** CCT diagram – heating at 1173 K

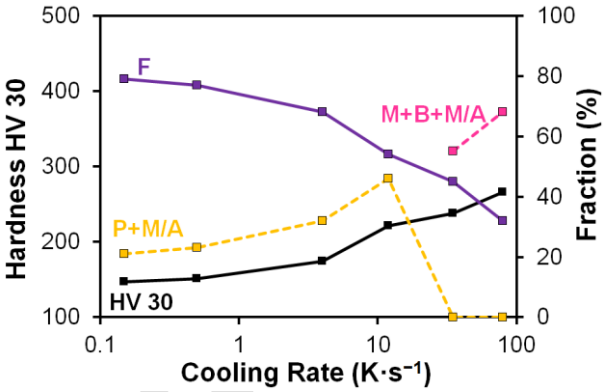


**b)** DCCT diagram – heating at 1173 K

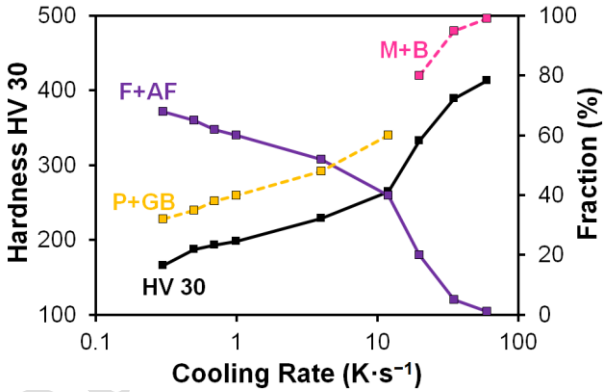


**c)** DCCT diagram – heating at 1553 K

**Fig. 10** Dependence of hardness HV 30 and fractions of austenite decomposition products on the cooling rate

Local microstructure inhomogenities observed especially in the specimens cooled at low cooling rates can be a consequence of either heterogeneity in the prior austenite grain size or the chemical heterogeneity of austenite. Micrographs in **Fig. 11** show the local occurrence of the M/A component (granular bainite) in the matrix formed by a mixture of ferrite and pearlite. Results of microhardness evaluation prove significantly higher hardness of granular bainite as compared to ferrite. Prior austenite grains after heating at the temperature of 1173 K were fine and homogeneous. Grain size distribution was not analyzed but the mean grain diameter, as determined from 200 measured values, was 9.9 μm with the standard deviation of 2.8 μm only (data in the interval from 4 to 18 μm). Granular bainite in Fig. 11b is not a consequence of the local presence of the coarse prior austenite grain. It is a result of an interdendritic microsegregation which could not be completely eliminated by the laboratory hot rolling and heat treatment. These areas are enriched by carbon, manganese and silicon. Both carbon and manganese have a significant effect on hardenability of steels.

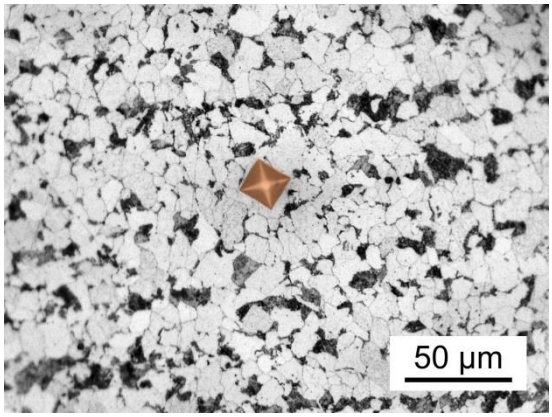


**a)** ferrite and pearlite microstructure; the average microhardness of ferrite: HV 0.05 = 153

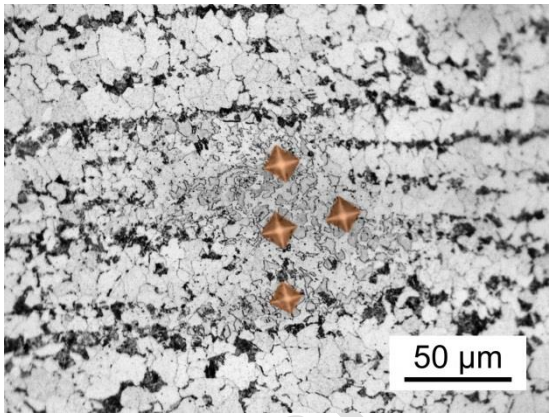


**b)** an island of granular bainite containing M/A islands; the average microhardness of bainite: HV 0.05 = 341

**Fig. 11** Local microstructure and microhardness heterogeneity after cooling at the rate of 1 $K \cdot s^{-1}$ – CCT diagram, heating at 1173 K

It is evident from **Fig. 12** that microhardness of a mixture of acicular ferrite and pearlite is higher about approx. 30 % in comparison to the allotriomorphic ferrite. Acicular ferrite is formed by the displacive mechanism and that is why it is oversaturated by carbon. It is harder than allotriomorphic ferrite [46, 47].

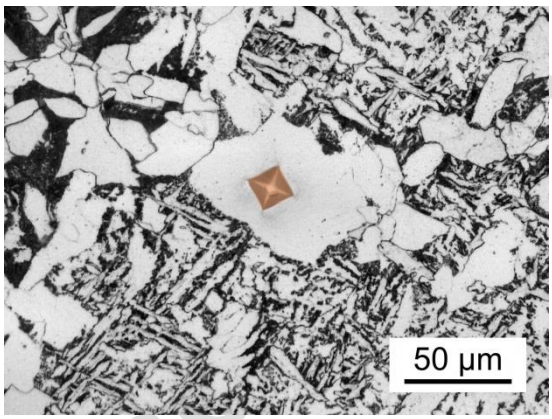


**a)** polygonal ferrite, HV 0.05 = 201

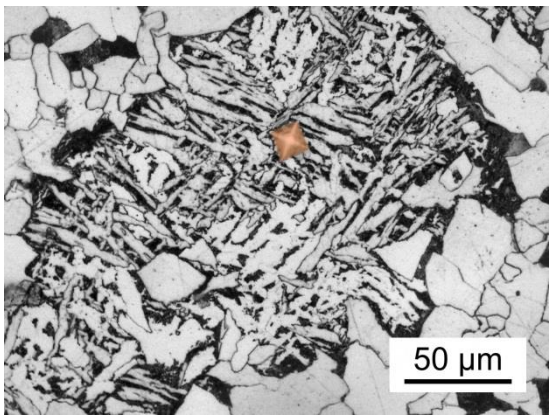


**b)** acicular ferrite and pearlite, HV 0.05 = 267

**Fig. 12** Microhardness of allotriomorphic ferrite and acicular ferrite + pearlite; DCCT diagram – heating at 1553 K, cooling rate of 0.7 $K \cdot s^{-1}$

Graph in **Fig. 13** shows that microhardness of the dilatometer specimens for individual cooling rates is highest for the DCCT diagram after austenitization at 1553 K. It indicates the importance of dissolution of MX carbonitrides at this high temperature and subsequent re-precipitation of fine MX precipitates during plastic deformation at 1173 K.

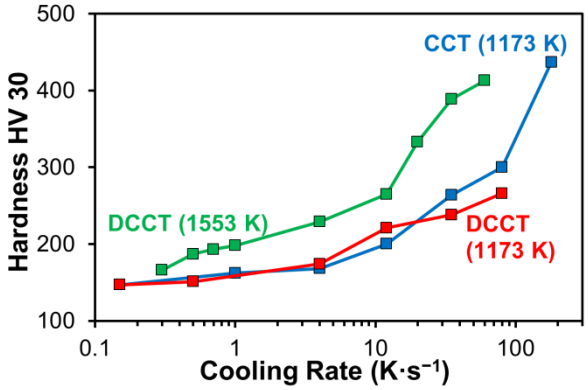


**Fig. 13** Effect of cooling rates and previous processing conditions on the hardness HV 30 of dilatometer specimens

### 3.3. Transformation diagrams

Graphs in **Figs. 14 – 16** demonstrate the continuous cooling transformation diagrams constructed using the data obtained by the dilatation curves analysis, metallography investigations and hardness evaluation. Symbols in these diagrams mean: Fs = Ferrite-start, Ps = Pearlite-start, Pf = Pearlite-finish, Bs = Bainite-start or Granular_bainite-start, Ms = Martensite-start. The positions of Ms curves under the Bs curves is typical for granular bainite. As shown in **Fig. 17**, the effect of austenite deformation at 1173 K on the kinetics of austenite decomposition is not significant. The effect of austenite plastic deformation at the relatively high temperature does not have a significant effect on the kinetics of austenite decomposition due to the austenite softening processes before phase transformations.

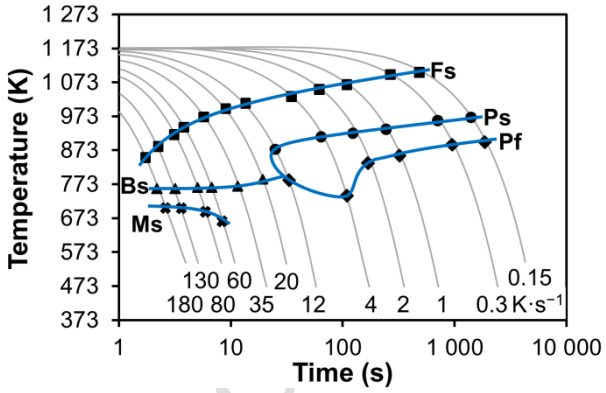


**Fig. 14** CCT diagram, heating at 1173 K

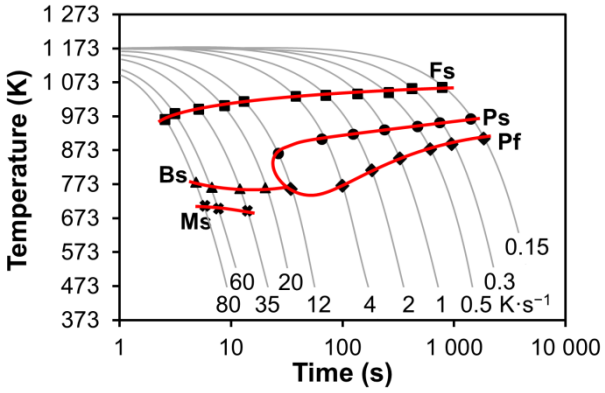


**Fig. 15** DCCT diagram, heating at 1173 K

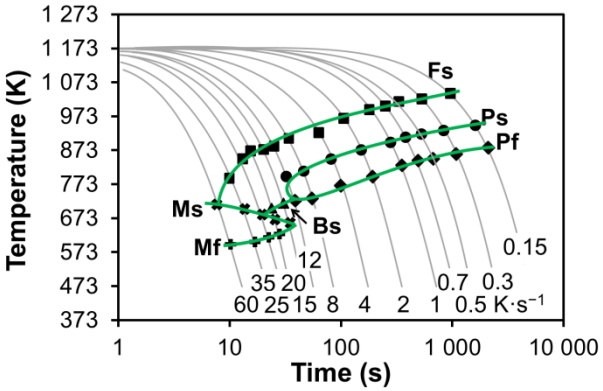


**Fig. 16** DCCT diagram, heating at 1553 K

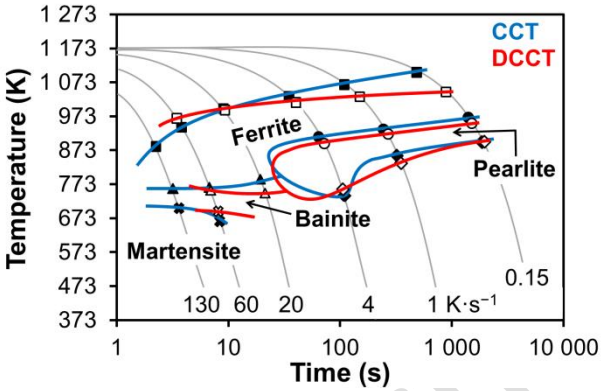


**Fig. 17** Superimposed CCT and DCCT diagrams, heating at 1173 K

Bainite transformation field in the DCCT (1553 K) diagram is much less pronounced than that in the CCT (1173 K) and DCCT (1173 K) diagrams. High heating temperature of 1553 K resulted in dissolution of MX carbonitrides in the as-cast microstructure and in the formation of coarse austenite grains. Subsequent deformation at 1173 K was accompanied by the deformation induced precipitation of fine MX particles [48] but the expected effect of the applied plastic deformation on refinement of the prior austenite grain size is small. Decomposition of austenite at moderate cooling rates resulted in the formation of a significant volume fraction of acicular ferrite. It has been reported that in the coarse austenite grains the intragranular acicular ferrite nucleates easier than bainite [33]. Bainitic ferrite laths nucleate at prior austenite grain boundaries. In the case of coarse prior austenite grains the area of grain boundaries per unit volume is small. It is expected that MX precipitates facilitate the heterogeneous nucleation of acicular ferrite in coarse austenite grains. That is why the formation of bainite in the coarse grained austenite is suppressed. On the other hand, martensite forms at high cooling rates and its formation is not preceded by the formation of acicular ferrite.

Graph in **Fig. 18** shows the superimposed DCCT transformation diagrams for both austenitization temperatures investigated. The kinetics of austenite→pearlite transformation is not significantly affected. Coarse prior austenite grains after heating at 1553 K result in a deep reduction of the Fs temperature at medium and high cooling rates. This is associated with the formation of acicular ferrite. The Fs temperature can be reduced by hundreds of Kelvins up to approx. 773 K.

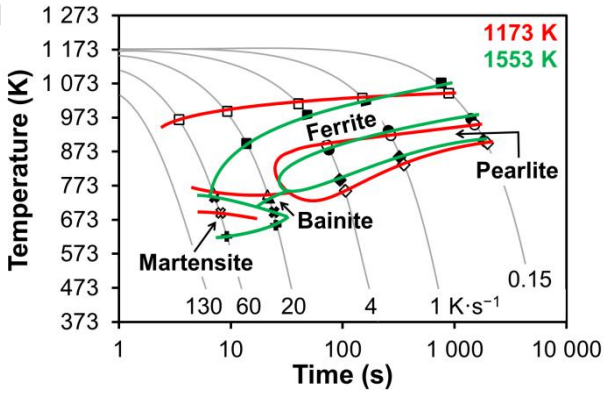


**Fig. 18** Superimposed DCCT diagrams – effect of the heating temperature 1173 K or 1553 K

## 4. DISCUSSION

The temperature-controlled rolling of seamless tubes is a rather specific technology which is characterized by long operation times affecting the precipitation processes and their interaction with the softening processes [49].

Microalloying elements are regarded to have a strong effect on microstructure evolution in HSLA steels during their thermo-mechanical treatment [50]. Their effects depend strongly on the stability and solubility of MX (where M = Nb, V, Ti; X = C, N) precipitates as a function of temperature. The principal mechanisms are grain size refinement and precipitation hardening due to the MX formation. In the steel investigated a full dissolution of MX particles during heating at 1553 K is expected. Size and distribution of MX particles re-precipitated during subsequent heating and deformation at 1173 K should be more efficient than those existing in the as-cast structure. In the case of specimens heated or heated and deformed at the temperature of 1173 K, most niobium rich MX particles are expected to be inherited from the initial microstructure [51, 52]. At this temperature only vanadium rich MX particles are expected to be dissolved. MX particles slow down the austenite recrystallization, increase the recrystallization stop temperature and limit the grain growth of austenite. Furthermore, additions of the strong carbide forming elements can reduce the temperature of austenite decomposition to ferrite.

In most cases, plastic deformation of austenite shifts the Fs temperature up and the C-curves for both diffusion-controlled transformations and bainite transformation are shifted to the left [20, 53]. However, Fig. 17 shows that the Fs temperature in the CCT and DCCT transformation diagrams for the investigated steel exhibit in the range of very slow cooling rates from 0.15 to 4 $K \cdot s^{-1}$ the opposite effect. This retardation of austenite→ferrite transformation at very slow cooling rates could have been caused by static recrystallization of deformed austenite, followed by a certain grain growth. This effect of plastic deformation on decomposition of austenite is not exceptional. Opiela et al. [54] studied the influence of austenite deformation on CCT diagrams for a steel containing 0.28 C – 1.41 Mn – 0.29 Si – 0.26 Cr – 0.22 Mo – 0.027Nb – 0.028 Ti – 0.019 V – 0.003 B (in weight %). Boron, if dissolved in the solid solution, has a positive effect on hardenability of steels. The austenitization temperature can influence the formation of coarse high temperature boron compounds [55]. Segregation of boron at austenite grain boundaries delays nucleation of allotriomorphic ferrite and decreases the critical cooling rate. Three transformation diagrams reported in the paper [54] involve the CCT diagram and the DCCT diagram after austenitization at the temperature of 1158 K and after 50% plastic deformation at the same temperature, respectively. Finally, the DCCT diagram after heating at the high temperature of 1473 K followed by plastic deformation at the temperature of 1373 K is shown. In both DCCT diagrams, the value of true strain was equal to 0.69 and the strain rate was 1 $s^{-1}$. Comparison of the individual diagrams shows that the effect of the high temperature austenitization is strong and results in the shift of the C-curves for diffusion-controlled transformations towards right. On the other hand, the effect of plastic deformation at the temperature of 1158 K is relatively weak and the Fs curve in the DCCT diagram lies slightly under the Fs curve for the CCT diagram. This is in agreement with the results presented in Fig. 17.

In Figs. 14 and 15 the Ms temperature descends with decreasing the cooling rate. Generally, the Ms temperature falls with increasing the content of carbon in the solid solution [56]. Precipitation of carbides in austenite before its decomposition results in an increase of the Ms temperature. On the other hand, in the deformed austenite a slight lowering of the Ms temperature can be explained by a carbon enrichment of the austenite regions adjacent to the bainite transformation products [20]. The value of deformation seems to be important as well. He et al. [57] found out that the Ms temperature first increased at small strains and then decreased at large strains. Nürnberger et al. [5] noticed the prevailing increase of the Ms temperature with the larger compressive deformation in some low-alloy steels. Decrease of the Ms temperature with decreasing the cooling rate observed in Figs. 14 and 15 can be explained by increasing

the ferrite fraction in microstructure with decreasing the cooling rate. The presence of the Ms curve under the Bs curve is generally associated with the formation of the M/A component in granular bainite.

The transformation diagrams obtained for the steel investigated were confronted with CCT/DCCT diagrams of similar steel grades available in the literature [6, 7]. **Figure 19** shows the CCT diagram of the steel containing 0.13 C – 1.53 Mn – 0.25 Si – 0.01 V – 0.043 Nb (in weight %) based on a combination of dilatometer tests and HAZ tests performed on the Gleeble 3800 simulator [7]. Test specimens were heated to the temperature of 1573 K at the rate of 200 $K \cdot s^{-1}$, followed by the very short dwell of 0.1 s. The cooling rates varied in the range from 0.5 to 120 $K \cdot s^{-1}$. In the CCT diagram, the same phase transformations were detected as in Fig. 14. Nevertheless, a detailed comparison of CCT diagrams in Figs. 14 and 21 shows that the C-curves for diffusional transformations as well for bainite transformation are in Fig. 21 shifted to longer times. This might have been caused by several reasons: the differences in chemical composition [58-60], the heating temperature (1553 K vs. 1573 K), and the prior austenite grain size [7, 61-64]. However, the transformation temperatures themselves show good agreement. Possible uncertainty may exist in microstructure interpretation in the field of bainite transformation. Bainite can be easily confused with acicular ferrite, which is often referred to as the bainitic ferrite [64-68].

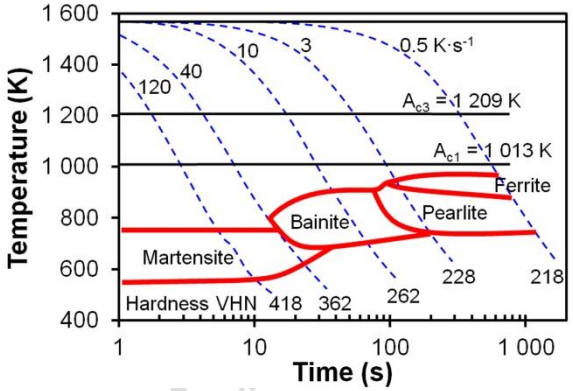


**Fig. 19** CCT diagram of a Nb-microalloyed steel constructed on the basis of combination of dilatometer and HAZ tests – according to [7]

Results of extensive work related to the design and modeling of the CCT/DCCT diagrams of HSLA steels with varying contents of Nb and Mo were published by Isasti et al. [6]. The experiments were carried out on the deformation dilatometer Bähr DIL805D after annealing of specimens at the temperatures of 1473 – 1523 K, ensuring dissolution of niobium rich MX precipitates. Phases and microstructural components in test specimens were classified in accordance with the ISIJ Bainite Committee notification [69]: polygonal ferrite (PF), lamellar pearlite (P), degenerated pearlite (DP), quasi-polygonal (or massive) ferrite (QF), granular ferrite (GF), bainitic ferrite (BF) and martensite (M). Similar classification of austenite decomposition products in low carbon steels can be found in [70]. The M/A islands were interpreted as part of the QF and GF components. The chemical composition of the 28NbHC steel grade was as follows: 0.11 C – 0.99 Mn – 0.23 Si – 0.028 Nb – 0.006 N (in weight %). It is very close to the steel investigated in this paper. The CCT diagram of the 28NbHC steel grade is shown in **Fig. 20.**

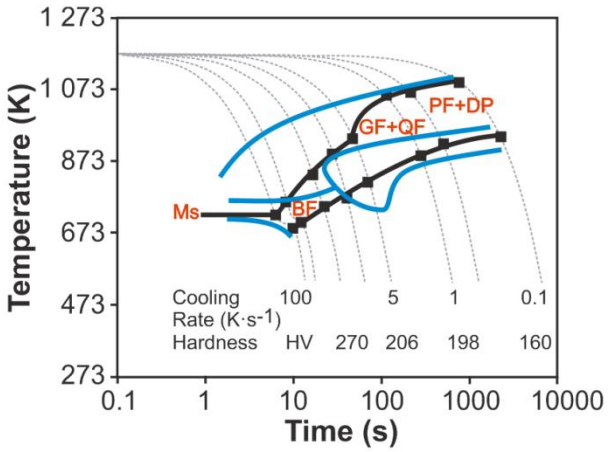


**Fig. 20** CCT diagram of the 28NbHC steel grade; black points and curves [6] superimposed with the CCT diagram presented in Fig. 14 – blue curves

The prior austenite grain size was evaluated as 44 μm. For a better comparability, the CCT diagram in Fig. 22 was superimposed by the CCT (1173 K) diagram presented in Fig. 14. Good matching of the Fs and Pf curves in both CCT diagrams is evident in the area of very slow cooling rates. The increase in the cooling rate results in a growing discrepancy between the Fs and Pf temperatures in both CCT diagrams. At high cooling rates the products of austenite decomposition are different. In the CCT diagram for the 28NbHC steel grade the BF region is observed but in the CCT diagram developed in this paper the bainite transformation is suppressed due to an intensive formation of ferrite. The shift of the ferrite region to shorter times could be explained by the finer prior austenite grain size (10 μm vs. 44 μm). The Ms temperatures in both CCT diagrams are approximately matching. It is generally accepted that if the formation of martensite is not preceded by precipitation of carbides in austenite or by the formation of ferrite, then the Ms temperature should not change with the cooling rate. The fraction of ferrite in the steel investigated in this paper increases with the decreasing the cooling rate (see Tab. 1) and is associated with a drop of the Ms temperature.

## 5. CONCLUSIONS

- Three continuous cooling transformation diagrams of the CCT or DCCT type were developed for the Cr, Nb, V and N-bearing HSLA steel intended for the seamless tubes production. Previous plastic deformation (with the true strain of 0.35) at the temperature of 1173 K influenced the austenite decomposition only slightly.
- The effect of the austenitization temperature (1173 K vs. 1553 K) and the prior austenite grain size (approx. 10 μm vs. more than 200 μm) on the phase transformations was enormous. Decomposition of coarse-grained austenite at the medium and high cooling rates favored the formation of acicular ferrite at the expense of allotriomorphic ferrite. It was accompanied by the decrease of the Ferrite-start temperature by hundreds of Kelvins.
- The DCCT diagrams developed in this paper can be applied in a seamless tube rolling mill for the prediction of austenite decomposition products and hardness of the rolled products after their cooling from the finish rolling temperature. The CCT diagram can be used for optimization of the quality heat treatment of seamless tubes.

**Acknowledgment**

*The implemented experimental work was supported by three grant projects: CZ.1.05/2.1.00/19.0387 and SP2019/86 (Ministry of Education, Youth and Sports of the Czech Republic), and FV10253 (Ministry of Industry and Trade of the Czech Republic).*

**References**

[1] I. Tamura, C. Ouchi, H. Sekine, T. Tanaka, Thermomechanical processing of high-strength low-alloy steels, Butterworths, Boston, 1988, p. 248.
[2] H.J. McQueen, Mater. Sci. Forum, 539–543 (2007) 4397–4404.
[3] P. Kawulok, R. Kawulok, I. Schindler, S. Rusz, J. Kliber, P. Unucka, K.M. Čmiel, Metalurgija, 53 (2014) 299-302.
[4] J. Trzaska, L.A. Dobrzański, J. Mater. Process. Technol., 192 (2007) 504-510.
[5] F. Nürnberger, O. Grydin, M. Schaper, F.W. Bach, B. Koczurkiewicz, A. Milenin, Steel Res., 81 (2010) 224-233.
[6] N. Isasti, P.M. García-Riesco, D. Jorge-Badiola, M. Taheri, B. López, P. Uranga, ISIJ Int., 55 (2015) 1963-1972.
[7] S. Kumar, S.K. Nath, V. Kumar, Mater. Des., 90 (2016) 177-184.
[8] A. Grajcar, W. Zalecki, R. Kuziak, J. Achiev. Mater. Manuf. Eng., 45 (2011) 115-124.
[9] E. Rożniata, R. Dziurka, Arch. Metall. Mater., 60 (2015) 497-502.
[10] C. Mesplont, Phase transformations and microstructure - mechanical properties relations in Complex Phase high strength steels, Ph.D. thesis, Gent University, Gent, 2002, p. 234.
[11] J. Trzaska, A. Jagiełło, L.A. Dobrzański, Arch. Mater. Sci. Eng., 39 (2009) 13-20.
[12] F. Nürnberger, O. Grydin, Z. Yu, M. Schaper, Metallurgical and Mining Industry, 3 (2011) 79-86.
[13] R. Kawulok, I. Schindler, P. Kawulok, S. Rusz, P. Opěla, Z. Solowski, K.M. Čmiel, Metalurgija, 54 (2015) 473-476.
[14] R. Kawulok, I. Schindler, P. Kawulok, S. Rusz, P. Opěla, J. Kliber, Z. Solowski, K.M. Čmiel, P. Podolínský, M. Mališ, Z. Vašek, F. Vančura, Metalurgija, 55 (2016) 357-360.
[15] S. Rusz, I. Schindler, P. Kawulok, R. Kawulok, P. Opěla, J. Kliber, Z. Solowski, Metalurgija, 55 (2016) 655-658.
[16] I. Schindler, S. Rusz, P. Opěla, J. Rusz, Z. Solowski, K.M. Čmiel, Met. Mater., 55 (2017) 229-236.
[17] P. Kawulok, I. Schindler, J. Mizera, R. Kawulok, S. Rusz, P. Opěla, M. Olszar, K.M. Čmiel, Arch. Metall. Mater., 63 (2018) 907-914.
[18] P. Kawulok, P. Podolinský, P. Kajzar, I. Schindler, R. Kawulok, V. Ševčák, P. Opěla, Arch. Metall. Mater., 63 (2018) 1743-1748.
[19] R. Bengoechea, B. López, I. Gutierrez, Metall. Mater. Trans. A, 29 (1998) 417-426.
[20] J. Adamczyk, M. Opiela, J. Mater. Process. Technol., 157–158 (2004) 456–461.
[21] V.M. Khlestov, E.V. Konopleva, H.J. McQueen, Mater. Sci. Technol., 18 (2002) 54-60.
[22] S.B. Yin, X.J. Sun, Q.Y. Liu, Z.B. Zhang, J. Iron Steel Res. Int., 17 (2010) 43-47.
[23] D. Jandová, L. Vadovicová, Proc. XIII International Metallurgical & Material Conference Metal 2004, 18. – 20. 5. 2004, Hradec nad Moravicí, The Czech Republic, 2004, paper no. 223.
[24] M. Gao, H. Gu, F. Xiao, B. Liao, G. Qiao, K. Yang, Y. Shan, J. Mater. Sci. Technol., 20 (2004) 89-91.
[25] A.A. Kruglova, V.V. Orlov, E.I. Khlusova, Met. Sci. Heat Treat., 49 (2007) 556-560.
[26] L. Strojeva, D. Ponge, R. Kaspar, D. Raabe, Acta Mater., 52 (2004) 2209-2220.
[27] R. Kawulok, P. Kawulok, I. Schindler, P. Opěla, S. Rusz, V. Ševčák, Z. Solowski, Arch. Metall. Mater., 63 (2018) 1735-1741.

[28] I. Schindler, J. Němec, P. Kawulok, R. Kawulok, V. Ševčák, P. Opěla, S. Rusz, Kovove Mater., 56 (2018) 163-170.
[29] L.X. Du, H.L. Yi, H. Ding, X.H. Liu, G.D. Wang, J. Iron Steel Res. Int., 13 (2006) 37-39.
[30] A. Timoschenkov, P. Warczok, M. Albu, J. Klarner, E. Kozeschnik, G. Gruber, C. Sommitsch, Steel Res. Int., 85 (2014) 954-967.
[31] Z. Zhao, C. Liu, Y. Liu, D.O. Northwood, J. Mater. Sci., 36 (2001) 5045-5056.
[32] R. Kaspar, U. Lotter, Ch. Biegus, Steel Res., 65 (1994) 242-247.
[33] H.K.D.H. Bhadeshia, Bainite in steels. Transformations, Microstructure and Properties, 2nd ed., IOM Communications Ltd., London, 2001, p. 454.
[34] H.L. Yi, L.X. Du, G.D. Wang, X.H. Liu, J. Iron Steel Res. Int., 13 (2006) 36-39.
[35] H.Z. Wang, P. Yang, W.M. Mao, F.Y. Lu, J. Alloys Compd., 558 (2013) 26-33.
[36] S.J. Lee, Y.K. Lee, Mater. Sci. Forum, 475-479 (2005) 3169-3172.
[37] R.A. Farrar, Z. Zhang, S.R. Bannister, G.S. Barritte, J. Mater. Sci., 28 (1993) 1385-1390.
[38] M.M. Aranda, B. Kim, R. Rementeria, C. Capdevila, C. García de Andrés, Metall. Mater. Trans. A, 45 (2014) 1778-1786.
[39] C.A. Däcker, O. Karlsson, C. Luo, K. Zhu, J.L. Collet, M. Green, P. Morris, R. Kuziak, N. Kwiaton, C. Stallybrass, Z.I. Olano, Bainitic hardenability – effective use of expensive and strategically sensitive alloying elements in high strength steels (BainHard), Publications Office of the European Union, Luxembourg, 2012, p. 146.
[40] S.J. Lee, Y.K. Lee, Mater. Des., 29 (2008) 1840-1844.
[41] S.J. Lee, J.S. Park, Y.K. Lee, Scr. Mater., 59 (2008) 87-90.
[42] H.S. Yang, H.K.D.H. Bhadeshia, Scr. Mater., 60 (2009) 493-495.
[43] S. Turteltaub, A.S.J. Suiker, Int. J. Solids Struct., 43 (2006) 7322-7336.
[44] W.L. Roberts, Hot rolling of steel, Marcel Dekker, INC., New York, 1983, p. 644.
[45] Y. Seillier, I. Schindler, R. Kawulok, P. Opěla, R. Turoň, R. Jurča, Proc. XXVI International Conference on Metallurgy and Materials – Metal 2017, 24. – 26. 5. 2004, Brno, The Czech Republic, 2004, p. 375-382.
[46] W.L. Costin, O. Lavigne, A. Kotousov, Mater. Sci. Eng. A, 663 (2016) 193-203.
[47] Y. Gu, G.Y. Qiao, D.Y. Wu, B. Liao, F.R. Xiao, Mater. Chem. Phys., 183 (2016) 506-515.
[48] B. Dutta, E.J. Palmiere, C.M. Sellars, Acta mater., 49 (2001) 785–794.
[49] R.N. Carvalho, M.A.C. Ferreira, D.B. Santos, R. Barbosa, Mater. Sci. Forum, 715-716 (2012) 988-993.
[50] J.C. Villalobos, A. Del-Pozo, B. Campillo, J. Mayen, S. Serna, Metals, 8 (2018) Article Number: 351.
[51] S.G. Hong, H.J. Jun, K.B. Kang, C.G. Park, Scripta Mater., 48 (2003) 1201–1206.
[52] H.Y. Lee, K.-S. Park, J.H. Lee, Y.-U. Heo, D.-W. Suh, H.K.D.H. Bhadeshia, ISIJ Inter., 54 (2014) 1677-1681.
[53] A. Grajcar, W. Kwaśny, W. Zalecki, Mater. Sci. Technol., 31 (2015) 781-794.
[54] M. Opiela, W. Zalecki, A. Grajcar, J. Achiev. Mater. Manufact. Eng., 51 (2012) 78-89.
[55] M. Deepa, G. Sahoo, S.K. Dhua, J. Min. Metall. Sect. B-Metall., 54 B (2018) 339–347.
[56] S.M.C. van Bohemen, Mater. Sci. Technol., 28 (2012) 487-495.
[57] B.B. He, W. Xu, M.X. Huang, Mater. Sci. Eng. A, 609 (2014) 141-146.
[58] H.J. Xie, X.C. Wu, Y.A. Min, J. Iron Steel Res. Int., 15 (2008) 56-61.
[59] J. Calvo, I.H. Jung, A.M. Elwazri, D. Bai, S. Yue, Mater. Sci. Eng. A, 520 (2009) 90-96.
[60] W. Vermeulen, S. Zwaag, P. Morris, T. Weijer, Steel Res., 68 (1997) 72-79.
[61] A.H. Seikh, M.S. Soliman, A.A. Majid, K. Alhajeri, W. Alshalfan, Adv. Mater. Sci. Eng., 2014, Article ID 246143.

[62] M.I. Onsøien, M. M'Hamdi, A. Mo, Am. Weld. Soc. J., 88 (2009) 1S-6S.
[63] Y. Wang, Y. Zheng, T. Wang, B. Liao, L. Liu, Adv. Mater. Res., 750-752 (2013) 380-384.
[64] R. Shukla, S.K. Ghosh, D. Chakrabarti, S. Chatterjee, Mater. Sci. Eng., A, 587 (2013) 201-208.
[65] J.L. Dossett, H.E. Boyer, Practical heat treating, 2nd ed., ASM International, Materials Park Ohio, 2006, p. 296.
[66] J. Lin, D. Balint, M. Pietrzyk, Microstructure Evolution in Metal Forming Processes, Woodhead Publishing Limited, Cambridge, 2012, p. 384.
[67] L. Zhongqiu, F. Jian, Z. Yong, Y. Zexi, Energy Procedia, 16 (2012) 444-450.
[68] M. Nikravesh, M. Naderi, G.H. Akbari, W. Bleck, Mater. Des., 84 (2015) 18–24.
[69] T. Araki, Atlas for Bainitic Microstructures, 1st ed., ISIJ, Tokyo,1992.
[70] G. Krauss, STEELS Processing, Structure, and Performance, 2nd ed., ASM International, Materials Park Ohio, 2015, p. 704.